



# The developmental gene Chordin is amplified and expressed in human cancers

Eric Sosa <sup>a</sup> and Edward M. De Robertis <sup>b</sup>

<sup>a</sup>Department of Genetics, Albert Einstein College of Medicine, Bronx, NY, USA; <sup>b</sup>Department of Biological Chemistry, David Geffen School of Medicine, University of California, Los Angeles, CA, USA

## ABSTRACT

Chordin (CHRD) is a secreted protein important in early development, yet a role for CHRD in human disease has not been identified. In this study we investigated CHRD in cancer and normal adult tissues using the wealth of genome-wide data available in public databases. We found that Chordin is amplified in the DNA of specific cancers such as lung squamous cell and others, although copy number variation did not strictly correlate with higher mRNA expression. In some cancers, such as renal and stomach carcinomas, increased CHRD expression significantly correlated with poor survival. In normal adult human tissues, CHRD mRNA was highest in hepatocytes. Crossveinless-2/BMPER, a component of the Chordin morphogenetic pathway expressed at the opposite side in embryos, was expressed in liver stellate cells. This raises the intriguing possibility that a BMP gradient might be established in the extracellular matrix of the space of Disse that surrounds portal sinusoid capillaries.

## ARTICLE HISTORY

Received 26 January 2023  
Revised 19 May 2023  
Accepted 19 May 2023

## KEYWORDS

Bone morphogenetic proteins; Chordin; Crossveinless 2; hepatocytes; lung squamous cell carcinoma; renal carcinoma; stellate cells; stomach carcinoma; scRNA-seq; TCGA

## Introduction

Chordin (CHRD) is a Bone Morphogenetic Protein (BMP) antagonist that plays a crucial role during development. Isolated initially from the Spemann organizer in the dorsal region of the *Xenopus* gastrula, CHRD protein is profusely secreted and is required for the inductive activities of transplanted Spemann organizer tissue.<sup>1–3</sup> CHRD binds BMPs in the extracellular space and prevents them from binding to their cognate receptors.<sup>4</sup> CHRD is a reversible inhibitor of BMPs, which is cleaved at two specific sites by Tolloid metalloproteinases releasing active BMP in the ventral side of the embryo.<sup>5</sup> The CHRD/Tolloid/BMP morphogenetic pathway establishes a dorsal-ventral gradient of BMP signaling which, remarkably, spans the entire embryo in most bilateral animal embryos, and even in the cnidarians.<sup>6,7</sup>

At the opposite pole of the embryo, the Crossveinless-2 (CV2) protein, renamed BMP Binding Endothelial Regulator (BMPER) in humans, has a structure related to that of CHRD.<sup>8</sup> CHRD binds BMP through four Cysteine-rich von Willebrand factor C (vWF-C) domains, while BMPER/CV2 has five. The main difference is that while CHRD diffuses readily through the extracellular matrix, BMPER/CV2 remains tethered to glypicans on the plasma membrane through a vWF-D domain.<sup>9,10</sup> CV2 serves to concentrate CHRD/Tolloid/BMP complexes on the ventral side of the embryo, where they are readily cleaved by Tolloids releasing BMPs to achieve maximal BMP signaling.<sup>9</sup> The Chordin-CV2 regulatory gradient takes place not only in the gastrula embryo but also in organogenesis of the cross-veins of the *Drosophila* wing and the developing vertebral bodies of the mouse.<sup>11,12</sup> Despite the evolutionarily

conserved role of CHRD in development, surprisingly, this gene has not been associated with specific human diseases.

In this paper, we examine the expression of CHRD in human cancers and adult tissues making use of the plethora of genome-wide data available in databases such as the Human Protein Atlas (HPA), Cancer Genome Atlas (TCGA), cBio Cancer Genomics Portal (cBioPortal), Dependency Map (DepMap), and Genotype-Tissue Expression (GTEx) portals.<sup>13–17</sup> We found that the CHRD gene is specifically amplified in the DNA of lung squamous cell carcinoma, ovarian, uterine, and esophageal carcinoma. In the adult human, CHRD expression is highest in liver. Single-cell RNA-sequencing (scRNA-seq) showed that CHRD is synthesized in hepatocytes, while the related protein CV2/BMPER is expressed specifically in hepatic stellate (also known as Ito) cells, raising the possibility of a gradient of CHRD/BMP activity in normal liver tissue.

## Results and discussion

### CHRD is amplified in specific cancers

Available CHRD alteration frequencies were extracted from 4,417 patients across 11 TCGA studies in the cBioPortal for Cancer Genomics (Figure 1a). CHRD was amplified (in red) in 40% of patients in three independent lung squamous cell carcinoma studies, providing validation for CHRD amplification in this type of cancer (Figure 1a). Lung squamous cell carcinoma patients harbored few CHRD point mutations (in green), suggesting amplification as the primary mode of CHRD involvement in cancer. CHRD was amplified to a lesser degree in patients with cutaneous squamous cell carcinoma and pan-

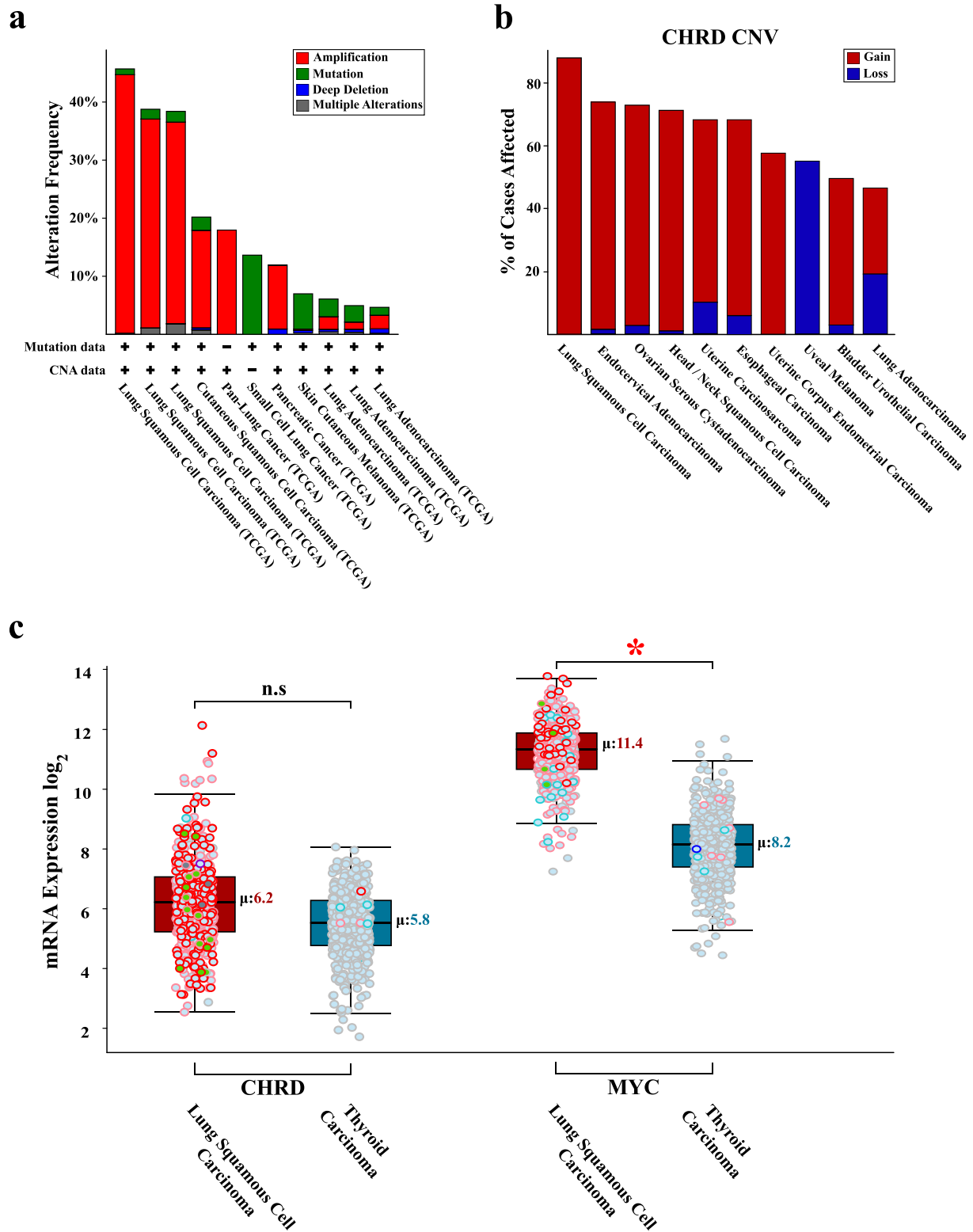


**Figure 1.** CHRD amplification in cancer does not correlate with higher mRNA expression. (a) Alteration frequencies indicate that CHRD DNA amplification is most common across pulmonary cancer subtypes. CHRD amplification was observed across multiple cancers except skin cutaneous melanoma and small cell lung cancer. This data was extracted from the cBioportal for Cancer Genomics and encompasses 4,417 patients across 11 TCGA studies. (b) A diversity of cancers harbor gain-of-function CHRD CNVs in 3,968 patients from 33 TCGA studies. CHRD CNVs are primarily gain-of-function with uveal melanoma serving as the only exception. (c) Chordin amplification is not significantly associated with increased mRNA expression in a subset of lung squamous cell carcinoma. Lung squamous cell carcinoma, which possesses high CHRD DNA amplification (red circles), had comparable CHRD mRNA expression compared to tumors with infrequent amplification (thyroid carcinoma). This pattern differs from what is observed in a well-established amplified oncogene, MYC, in which DNA amplification correlates with higher mRNA expression. In these data from TCGA, red and blue circles in the boxplot indicate the presence or absence of amplification, respectively. The black center line denotes the median value (50<sup>th</sup> percentile), while the red and blue boxes contain the 25<sup>th</sup> to 75<sup>th</sup> percentiles of the dataset. The black whiskers denote the 5<sup>th</sup> and 95<sup>th</sup> percentiles, and values beyond these upper and lower bounds are considered outliers. The single red asterisk indicates a p-value <.05 obtained via two-tailed Student's t-test.

lung cancer ( $\approx 20\%$  of patients). Interestingly, CHRD was mutated but not amplified in small cell lung cancer, suggesting differing roles for CHRD between pulmonary cancer subtypes. Pancreatic cancer and lung adenocarcinoma patients had a lower rate ( $<15\%$ ) of CHRD copy number variations (CNV), with pancreatic cancers primarily harboring CHRD amplification, and lung adenocarcinomas having equal proportions of CHRD point mutations and amplification (Figure 1a).

CHRD copy number variations (CNVs) were further analyzed in the genomes of 3,968 cancer patients across 33 TCGA studies available in the NCI Genomic Data Commons portal (Figure 1b). The majority of CHRD CNVs resulted in gain (in red) of chromosomal material, with uveal melanoma as the sole exception. Lung squamous cell carcinoma patients possessed the greatest number of CHRD gain CNVs (88% of all patients), while 70–75% of endocervical adenocarcinoma, ovarian serous cystadenocarcinoma, neck squamous cell carcinoma, uterine carcinoma, and esophageal carcinoma patients presented CHRD gains in CNVs. Uterine corpus endometrial carcinoma patients exclusively had CHRD gain CNVs (58%), in contrast to uveal melanoma patients who exclusively had CHRD loss CNVs (55%). Lung adenocarcinoma patients were the only group with an equal proportion of CHRD gain and loss CNVs. We conclude that the majority of CHRD CNVs are from the gain category, implicating CHRD amplification in specific types of cancers.

### **CHRD amplification does not correlate with higher mRNA expression**

We next searched whether copy number amplification of CHRD expression correlated with increased mRNA expression. The correlation between mRNA expression and DNA amplification was analyzed in 982 samples from lung squamous and thyroid carcinoma TCGA studies (Figure 1c). Lung squamous cell carcinoma was chosen due to its high frequency of CHRD amplification (red circles), while thyroid carcinoma was selected because of its infrequent CHRD amplification. The average CHRD mRNA expression in lung squamous cell carcinoma was 73 RPKM ( $\log_2 = 6.2$ ) with the 25<sup>th</sup> and 75<sup>th</sup> percentile defined by 37 RPKM ( $\log_2 = 5.2$ ) and 128 RPKM ( $\log_2 = 7$ ), respectively. Samples with CHRD expression above 861 RPKM ( $\log_2 = 9.75$ ) were considered significant outliers, of which there were nine samples. Similarly, the average CHRD expression in thyroid carcinoma was 56 RPKM ( $\log_2 = 5.8$ ) with the 25<sup>th</sup> and 75<sup>th</sup> percentile defined by 26 RPKM ( $\log_2 = 4.7$ ) and 74 RPKM ( $\log_2 = 6.22$ ), respectively. Thyroid carcinoma samples with CHRD expression above 268 RPKM ( $\log_2 = 8.07$ ) were considered significant outliers, of which there were 0 samples. Similar CHRD expression in the presence and absence of amplification suggested that CHRD amplification is not correlated with higher mRNA expression (Figure 1c, plots on the left side). In contrast, DNA amplification of the well-established oncogene MYC in the same lung squamous cell carcinomas significantly correlated with higher mRNA expression (Figure 1c, right side box plots). Lung squamous cell carcinoma possessed a significantly higher MYC mRNA expression of 2,702 RPKM ( $\log_2 = 11.4$ ) compared to thyroid carcinoma with an average MYC mRNA expression of 294

RPKM ( $\log_2 = 8.2$ ) ( $p < .05$ , two-tailed Student's t-test). From this comparison with MYC, we conclude that CHRD does not behave as a standard oncogene.

### **High CHRD expression correlates with decreased survival in renal and stomach carcinomas**

We next examined whether CHRD expression levels correlated with cancer survival according to data available through the Human Protein Atlas (HPA).<sup>13</sup> Only pan-lung cancer data was available for lung cancer, and we were unable to ascertain specifically lung squamous cell carcinoma; differences in pan-lung survival were not significant. A different situation arose when we analyzed data for CHRD RNA expression and survival curves from 877 renal carcinoma patients (Figure 2a). The average CHRD expression in renal carcinoma was 1.8 FPKM, with the 75<sup>th</sup> percentile defined at 2.5 FPKM. Of the 877 patients, 259 were categorized into the “high expression” group due to their CHRD expression above the upper whisker (5.4 FPKM). The remaining 618 patients constituted the “low expression” group. The renal carcinoma Kaplan-Meier plot from patients with high and low CHRD expression had 5-year survival rates of 55% and 74%, respectively ( $p = 6.1 \times 10^{-7}$ ). The survival probability widens after 10 years, as patients with high and low CHRD expression experienced survival rates of 37% and 64%, respectively. Thus, survival analysis suggest that high CHRD mRNA expression is prognostic and unfavorable in renal carcinoma (Figure 2a).

We also examined survivability curves and CHRD RNA expression data from 354 stomach carcinoma patients (Figure 2b). The average CHRD expression was 1.4 FPKM, with the 75<sup>th</sup> percentile defined at 2.2 FPKM. Of the 354 patients, 188 were categorized into the “high expression” group since their CHRD expression values were above the 95<sup>th</sup> percentile (4.5 FPKM) and considered outliers. The remaining 166 patients constituted the “low expression” group. Survivability analysis of stomach carcinoma patients with high and low CHRD expression had 5-year survival rates of 23% and 52%, respectively ( $p = .0055$ ), suggesting that high CHRD expression has unfavorable prognosis. Unlike in renal carcinoma, the 10-year survival rate was comparable between high and low CHRD expression groups in stomach carcinoma. Notably, high CHRD expression was also significantly correlated with decreased survival in cervical, colorectal, pancreatic, and urothelial cancers. We conclude that high CHRD expression may serve as a negative prognosis marker in some cancers.

### **Single-cell CHRD expression in hepatocytes and BMPER/CV2 in hepatic stellate (Ito) cells suggests a possible BMP signaling gradient in adult liver tissue**

CHRD mRNA expression was assessed in a consensus dataset created by combining the HPA, GTEx, and FANTOM transcriptomic databases available through the HPA. Notably, CHRD expression was highest across gastrointestinal structures (liver, kidney, pancreas), neural tissues (cerebellum, cortex, hippocampus), and reproductive organs (cervix,

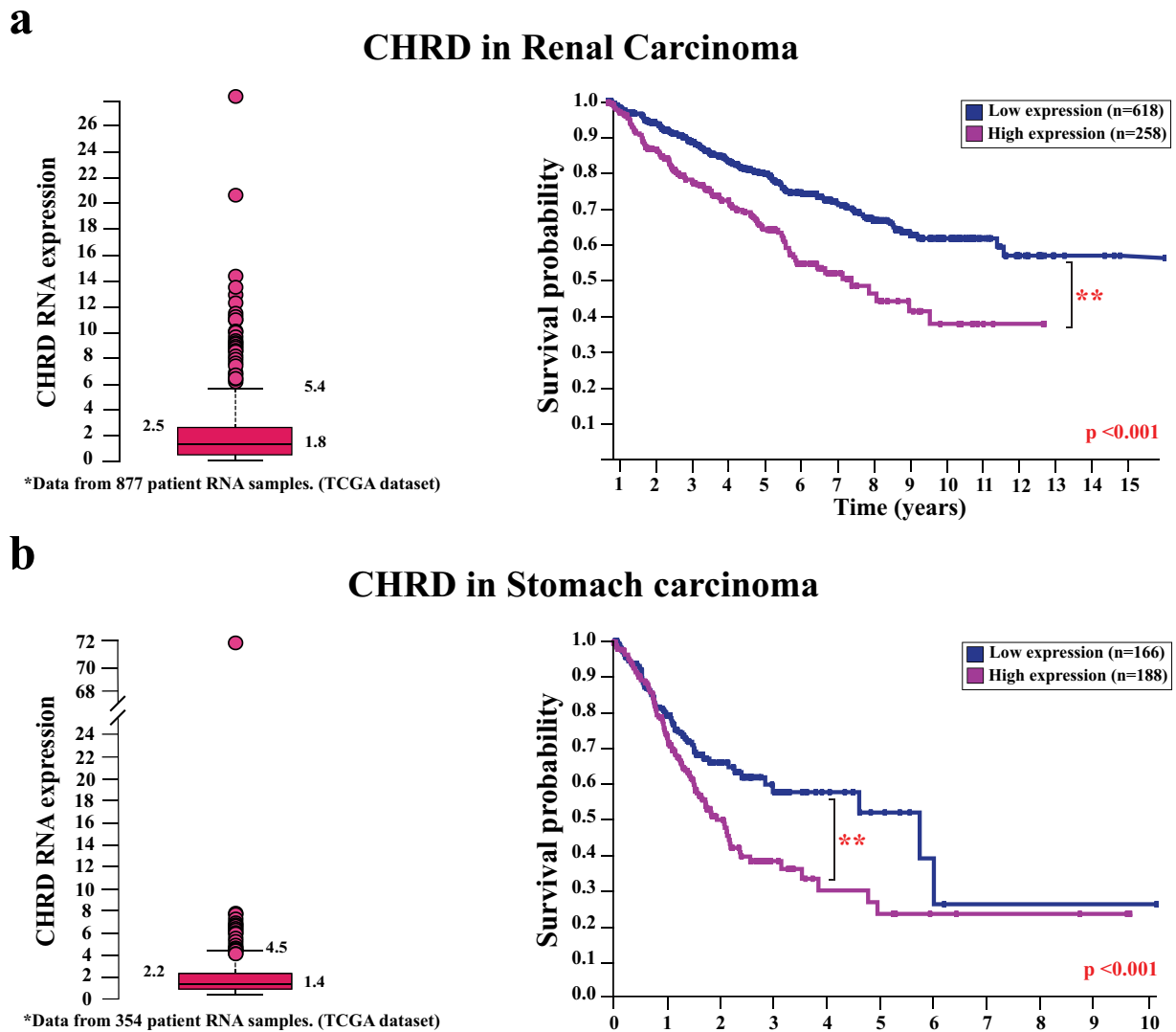


**Figure 2.** High CHRD expression correlates with decreased survival in renal and stomach carcinoma. (a) Box and whisker plot of CHRD RNA expression in renal carcinomas from 877 patients. Values above the black whisker (95<sup>th</sup> percentile) denote outliers and are colored in red. High CHRD RNA expression ( $\geq 6$  RPKM) is significantly correlated with decreased survival probability. Kaplan-Meier plots of patients with high and low CHRD expression possessed a 5-year survival rate of 55% and 74%, respectively ( $p = 6.1 \times 10^{-7}$ ). (b) Box and whisker plot of CHRD RNA expression in stomach carcinomas from 354 patients. High CHRD RNA expression ( $\geq 5$  RPKM) is significantly correlated with decreased survival probability. Kaplan-Meier plots of patients with high and low CHRD expression possessed a 5-year survival rate of 23% and 52%, respectively ( $p = .0055$ ). The double red asterisks indicate an obtained p-value  $< .001$  via two-tailed Student's t-test.

endometrium, ovary, vagina) in adult human tissues (Figure 3a). CHRD expression was highest in liver tissue at 130 normalized transcripts per million (nTPM). This was nearly 4-fold greater than its expression in cervix (40 nTPM) and endometrium (35 nTPM), while other organs had a CHRD expression of 20 nTPM or lower (Figure 3a).

Single-cell CHRD RNA expression was analyzed via UMAP (uniform manifold approximation and projection) in hepatic tissue (Figure 3b). CHRD expression was exclusively found in hepatocytes clusters, which are highlighted in the accompanying heatmap indicating their significant z-scores (Figure 3b). No other hepatic cell type possessed comparable or significant CHRD expression levels.

Interestingly, when single-cell CV2/BMPER expression (which marks the high side of the CHRD/BMP signaling gradient) was analyzed in the same hepatic cell samples, CV2/BMPER was strongly and significantly expressed in stellate cells (c-4) and absent in hepatocytes (Figure 3c). This is

represented in the UMAP plot by the presence of green dots and absence of blue ones. Kupffer cells (c-3) and B-cells (c-6) had low BMPER/CV2 expression, but these values were not statistically significant via z-score analysis (Figure 3c).

We conclude from this single-cell analysis of publicly available databases that Chordin is expressed at high levels by adult human hepatocytes. CV2/BMPER, which is normally expressed at the high end of BMP gradients during development, is specifically expressed in stellate cells. The possible physiological significance of this cellular distribution is examined below.

### Significance of the observations

While the role of CHRD protein and its regulation during early development has been extensively studied, there is a lack of information regarding its functional role in the adult. In this study, we analyzed *chrd* mutations in cancer. Data in DepMap

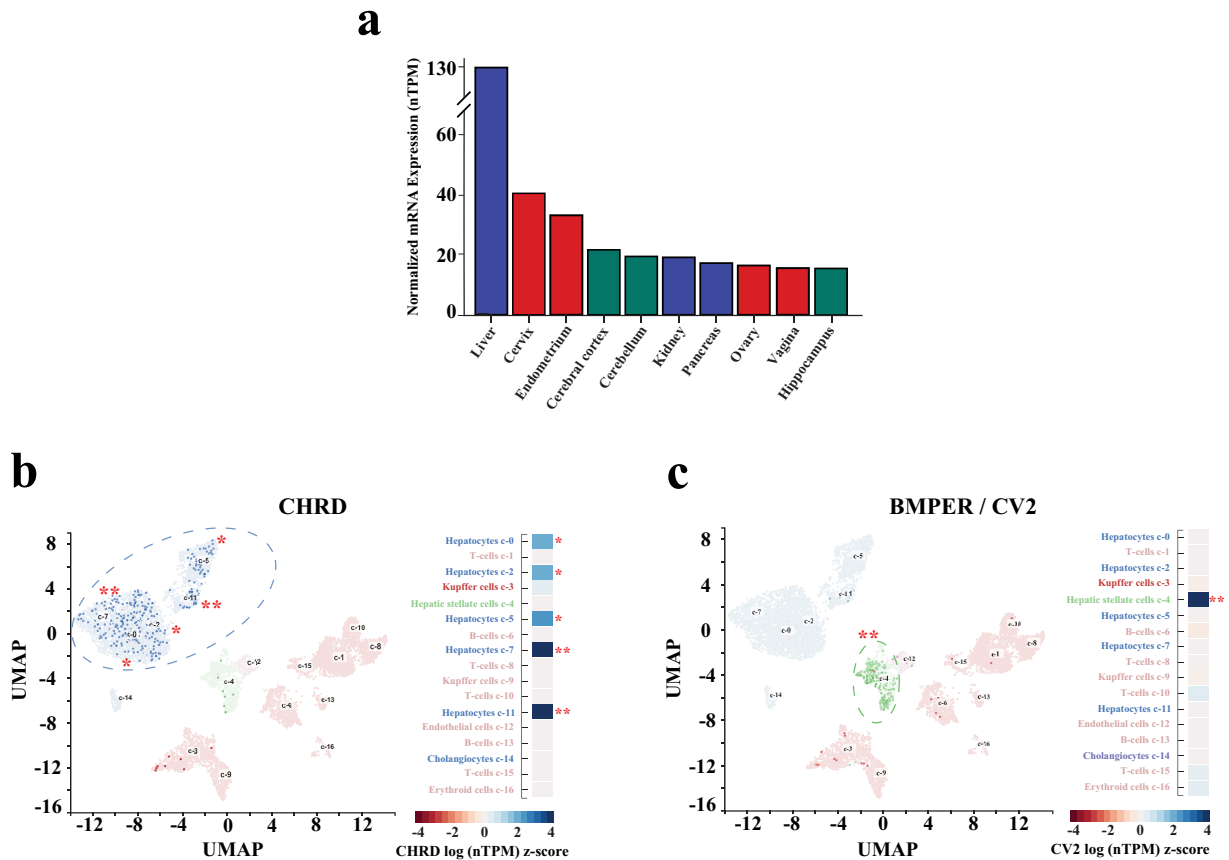


**Figure 3.** Single-cell CHRD expression in hepatocytes and BMPER/CV2 in hepatic stellate (Ito) cells suggests a BMP-signaling gradient in adult liver tissue. (a) Tissues with the highest reproducible CHRD mRNA expression include female reproductive structures (red bars), brain regions (green bars), and gastrointestinal organs (blue bars). Hepatic tissue contained the highest CHRD RNA expression with 130 nTPM. This consensus dataset was created by combining the HPA, GTEx, and FANTOM transcriptomic databases available through the Human Protein Atlas. (b) Single-cell hepatic CHRD expression data is limited exclusively to hepatocytes (blue coordinates) according to UMAP analysis. Z-scores were generated from single-cell RNA expression values and represented through a logarithmic heatmap. Cell types with a positive z-score possess significantly higher CHRD expression. Z-scores were converted to p-values to determine cell type CHRD expression significance \*  $p < .05$ , \*\*  $p < .01$ , indicated by red asterisks in the figure. (c) Conversely, CV2/BMPER single-cell expression is absent in hepatocytes and limited to mesenchymal stellate cells (green coordinates). Only stellate cells possessed a positive z-score reflecting a significantly higher CV2/BMPER expression. Single-cell RNA data was acquired from thousands of single-cell expression collections deposited in the Human Protein Atlas.

from solid tumors in 66,162 patients indicate that missense and silent mutations are distributed uniformly throughout the *chrd* gene and stop mutations are rare, suggesting that CHRD is unlikely to be a tumor suppressor. Interestingly, the *chrd* gene was found to be amplified in specific subsets of cancers, particularly in lung squamous cell carcinoma. (Figure 1). Kaplan-Meier plots of high and low *chrd* mRNA expression indicated that at least in some cancers, such as renal and stomach carcinoma (and cervical, colorectal, pancreatic, and urothelial cancers as well), high expression is correlated with significantly decreased survivability. We conclude that although *chrd* does not behave as a strong oncogene such as MYC, it may serve as a possible cancer biomarker, particularly if the increased mRNA levels were reflected in protein levels in blood samples, for which commercial detection kits exist.<sup>18</sup>

CHRD is expressed in adult tissues, with the highest levels reached in liver. Of interest for biomarker purposes, CHRD protein is found in blood plasma.<sup>19</sup> Using publicly available scRNA-seq data, we found that CHRD is specifically expressed in hepatocytes, which are the likely origin of the CHRD protein in the circulation. Chordin in blood might function in systemic cellular processes, such as hematopoiesis and immune or

inflammatory responses in which BMPs are involved.<sup>20</sup> In order to be secreted into the portal circulation sinusoid capillaries, proteins from hepatocytes must traverse the extracellular matrix located in the perisinusoidal space of Disse, where the liver stellate cells are located. Stellate cells are enigmatic endoderm-derived cells adjacent to the sinusoid portal capillaries.<sup>21</sup>

Our observation that CV2/BMPER, is expressed specifically in hepatic stellate cells (also called Ito cells), is potentially of physiological interest. In a number of developmental systems CV2 is expressed at the high end of BMP gradients, while the BMP antagonist Chordin is secreted from the low BMP end. In the *Xenopus* gastrula, CV2 is expressed in the ventral side while Chordin is secreted by dorsal Spemann-Mangold organizer tissue.<sup>6</sup> In the developing wing crossveins, which require maximal BMP signaling, CV2 is expressed in the crossvein itself.<sup>11</sup> As shown in Figure 4, Cv2 has structural similarities to Chordin, in particular vWF-C domains that act as BMP binding modules. Unlike Chordin/BMP complexes, CV2 is unable to diffuse and remains attached to the plasma membrane via glypicans in its cells of origin.<sup>10</sup> Since CV2 binds Chordin/BMP complexes and facilitates Chordin cleavage by Tolloid metalloproteinases, it functions as a sink that activates BMP signaling.<sup>9</sup>



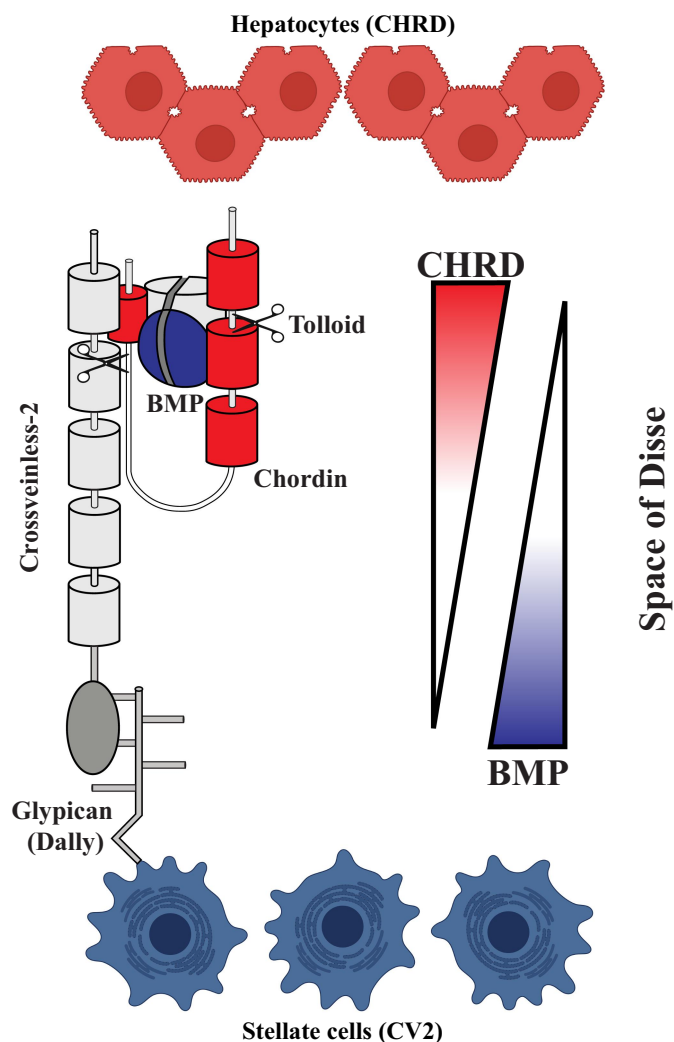


**Figure 4.** Diagram indicating the known biochemical functions of CHRD and CV2 in BMP morphogen signaling. Chordin is a protein that contains 4 VWF-C modules that bind BMPs. Twisted gastrulation is a co-factor that bridges the binding of BMP to Chordin modules and is shown as a dimer on top of BMP. At the high-BMP side of a BMP gradient the protein CV2, which has five VWF-C domains, binds to and concentrates BMP-Tsg-CHRD complexes, facilitating their cleavage by Tolloid metalloproteinases (shown by scissors). Once CHRD is cleaved, BMPs are liberated and signal through BMPR. While CHRD complexes readily diffuse between cells, CV2 contains a Vwf-D domain (shown here as an oval) that anchors it to Glypicans (called Dally in *Drosophila*) in the plasma membrane of the cells that secrete CV2. Because CHRD is expressed in hepatocytes (red) and CV2 in stellate cells (blue), we propose that these proteins may generate a BMP gradient within the perisinusoidal space of Disse in normal liver tissue.

The scRNA-seq data raise the exciting possibility that a CHRD/BMP morphogenetic gradient may be formed in the space of Disse in normal liver tissue. The genomic observations presented here indicate that CHRD may not only be involved in embryonic signaling gradients, but also in adult tissue homeostasis and cancer progression.

Understanding the prognostic relevance of CHRD expression across cancer subtypes may influence therapeutic decisions. Here, we have provided a clinical context for CHRD, analyzing its amplification status across cancers, and relating its mRNA expression to survival outcomes in gastric and renal carcinoma. Other chordin-like proteins have been investigated in the context of cancer. A study in breast cancer determined that Chordin-like 1 (CHRD-L1) –

a CHRD-like protein containing only 3 BMP-binding CR modules – acts as a negative regulator of malignant breast cancer phenotypes through BMP signaling inhibition.<sup>22</sup> They reported that high CHRD-L1 expression inhibited BMP-induced migration in breast cancer and was associated with prolonged survival outcomes.<sup>22</sup> Another report showed that CHRD inhibited BMP-induced migration in ovarian cancer cell lines.<sup>23</sup> In lung adenocarcinoma, CHRD-L1 was recently highlighted as a prognostic biomarker and promising therapy target.<sup>24</sup> Low CHRD-L1 correlated with poor clinicopathologic features and patient survival ( $p < .001$ ).<sup>24</sup> The study suggested that CHRD-L1 may serve as a potential therapy target via cell cycle regulation, and may improve the effectiveness of immunotherapy by regulating immune infiltration.<sup>24</sup> Another CHRD relative, Chordin-like 2 (CHRD-L2) has recently been suggested as a clinical biomarker that promotes cell proliferation through the YAP/TAZ pathway in gastric cancer.<sup>25</sup> Serum CHRD-L2 levels were distinctly upregulated in gastric cancers. The increased CHRD-L2 expression in serum was highest among poorly and undifferentiated gastric cancers, and significantly correlated with shorter patient survival.<sup>25</sup>

In conclusion, the present study indicates the potential clinical utility of CHRD as a biomarker that merits further exploration. Targeting CHRD in specific cancers may hold therapeutic promise. The results also suggest that a finely regulated CHRD-BMP-CV2 morphogenetic gradient could be a determinant of adult tissue homeostasis warranting further investigation.

## Materials and methods

### Online genomic resources

CHRD alteration frequencies from 4,417 patients across 11 TCGA studies were extracted and analyzed via the cBioPortal for Cancer Genomics. CHRD CNV data was acquired from the NCI Genomic Data Commons portal and included 3,968 patients across 33 TCGA studies. Barplots in Figure 1 were created using the package ggplot2 via the coding program R-Studio.<sup>26,27</sup> Box and whisker plots of CHRD and MYC amplification were created in R-Studio package ggplot2 from TCGA data acquired through the cBioPortal database. Logarithmic ( $\log_2$ ) fold-changes were used as input and acquired by the ratio of CHRD/MYC mRNA expression in lung/thyroid carcinoma over their expression in healthy tissue.

CHRD RNA expression in renal and stomach carcinoma was downloaded from the Human Protein Atlas (HPA) and reanalyzed via DESeq2 in R-Studio.<sup>28</sup> For reproducibility purposes, the data was screened to include only TCGA datasets. Both CHRD renal and stomach carcinoma datasets possessed a male-to-female bias of 2:1. Box and whisker plots were generated in the R-studio package BoxPlotR using fragments per kilobase of exon per million mapped fragments (FPKM) values as input.<sup>29</sup> Renal and stomach carcinoma Kaplan-Meier plot data were extracted from the Human Protein Atlas (HPA) and reanalyzed for significance in Excel via a two-tailed Student's t-test. Patients were classified into two expression groups, low and high, based on the FPKM value of CHRD.

We then examined the correlation between CHR D expression level and patient survival via Kaplan-Meier survival estimators.<sup>13</sup> Genes with a p-value lower than 0.001 in Kaplan-Meier analyses were defined as prognostic genes. Genes with a median expression less than FPKM 1 were lowly expressed and classified as un-prognostic.

CHR D mRNA expression in healthy tissues was extracted from the HPA. Normalized transcript per million (nTPM) values are from a consensus dataset created by combining the HPA, GTEx, and FANTOM transcriptomic databases using the internal normalization pipeline.<sup>13</sup> For the HPA and GTEx transcriptomics datasets, the average TPM value of all individual samples for each tissue was used to estimate CHR D expression level. TPM values of all samples within each data source were normalized separately using trimmed mean of *M* values (TMM) to allow for between-sample comparisons. The resulting normalized transcript expression values, denoted nTPM, were calculated for each gene in every sample.<sup>13</sup> The summary barplot was generated in R-Studio.

Hepatic CHR D scRNA-seq data was derived from a meta-analysis of literature on scRNA-sequencing from single cell databases including only healthy human tissue.<sup>13</sup> To ensure that single-cell dataset best represented their corresponding tissue, the following selection criteria were applied to avoid technical bias. First, only single-cell transcriptomic datasets based on Chromium single cell gene expression platform from 10× Genomics were considered. Secondly, only scRNA-sequencing performed on single-cell suspension from tissues without pre-enrichment of cell types were considered. Thirdly, only studies with > 4,000 cells and 20 million read counts were included, and only datasets whose pseudo-bulk transcriptomic expression profile is highly correlated with the transcriptomic expression profile of the corresponding HPA tissue bulk sample were analyzed.<sup>13</sup> CHR D and BMPER/CV2 hepatic scRNA-seq data was extracted from Bioproject GSE115469.<sup>30</sup>

CHR D and BMPER/CV2 scRNA-seq data was analyzed using Uniform Manifold Approximation and Projection (UMAP) analysis. UMAP is a dimensionality reduction tool used to visualize and understand high dimensional datasets by constructing a high dimensional graph of the data and then optimizing a low-dimensional graph to be as structurally similar as possible, allowing one to effectively visualize clusters of data points and their relative proximities.<sup>31</sup> UMAP analysis was used instead of the t-SNE analyses due to its increased speed and better preservation of global structure.<sup>31</sup> In the UMAP plots, each dot corresponds to an individual cell. UMAP plots were recreated in R-Studio by comparing CHR D and BMPER/CV2 sc-RNAseq values across all hepatic cell types in the library. The heatmaps in Figure 3 were recreated in R-Studio using scRNA-seq RPKMs of CHR D and BMPER/CV2 as input. Z-scores were obtained from the RPKMs by calculating the mean, variance, and standard deviation of CHR D and BMPER/CV2 expression in each cell type by using the gplots v3.0.1 package available in R-Studio.

## Disclosure statement

No potential conflict of interest was reported by the author(s).

## Funding

EAS was supported by the Ruth L. Kirschstein Predoctoral Individual National Research Service F31-Award: 1F31MH131380-01 and EMDR by NIH P20CA016042 to the University of California, Los Angeles Jonsson Comprehensive Cancer Center, and the Norman Sprague Endowment for Molecular Oncology. We thank Lauren V. Albrecht, Alyssa Hill, and Hiroki Kuroda from our laboratory for help in the initial stages of this project.

## ORCID

Eric Sosa  <http://orcid.org/0000-0001-5965-3477>

Edward M. De Robertis  <http://orcid.org/0000-0002-7843-1869>

## Statistical Analyses

Statistical analyses were performed in Excel (Microsoft Corp) and R-Studio via two-tailed Student's t-test. Differences of means were considered significant at a significance level of 0.05 ( $p \leq .05$ ).

## Data availability statement

The data that support the findings of this study are from the following resources available in the public domain: cBio Cancer Genomics Portal (<https://www.cbioportal.org/>), Dependency Map (<https://depmap.org/portal/>), Genotype-Tissue Expression portal (<https://gtexportal.org/home/>), Human Protein Atlas (<https://www.proteinatlas.org/>), and the Cancer Genome Atlas (<https://portal.gdc.cancer.gov/>).

## Abbreviations

BMP	Bone Morphogenetic Protein
BMPER	BMP Binding Endothelial Regulator
cBioPortal	cBio Cancer Genomics Portal
CHR D	Chordin
CNV	Copy Number Variation
CV2	Crossveinless-2
DepMap	Dependency Map
FPKM	Fragments per kilobase of exon per million mapped fragments
GTEx	Genotype-Tissue Expression
HPA	Human Protein Atlas
Ntpm	Normalized transcript per million
scRNA-seq	Single-cell RNA-sequencing
TCGA	The Cancer Genome Atlas
Tsg	Twisted gastrulation
UMAP	Uniform Manifold Approximation and Projection
vWF-C	von Willebrand factor C domain.

## References

1. Sasai Y, Lu B, Steinbeisser H, Geissert D, Gont LK, De Robertis EM. Xenopus chordin: a novel dorsalizing factor activated by organizer-specific homeobox genes. *Cell*. 1994;79(5):779–790. PMID: 8001117. doi:10.1016/0092-8674(94)90068-x.
2. Lee HX, Ambrosio AL, Reversade B, De Robertis EM. Embryonic dorsal-ventral signaling: secreted frizzled-related proteins as inhibitors of tolloid proteinases. *Cell*. 2006;124(1):147–159. PMID: 16413488. doi:10.1016/j.cell.2005.12.018.
3. Oelgeschläger M, Kuroda H, Reversade B, De Robertis EM. Chordin is required for the Spemann organizer transplantation phenomenon in Xenopus embryos. *Dev Cell*. 2003;4(2):219–230. PMID: 12586065. doi:10.1016/s1534-5807(02)00404-5.
4. Piccolo S, Sasai Y, Lu B, De Robertis EM. Dorsal-ventral patterning in Xenopus: inhibition of ventral signals by direct binding of

- chordin to BMP-4. *Cell*. 1996;86(4):589–598. PMID: 8752213. doi:10.1016/s0092-8674(00)80132-4.
5. Piccolo S, Agius E, Lu B, Goodman S, Dale L, De Robertis EM. Cleavage of Chordin by Xolloid metalloprotease suggests a role for proteolytic processing in the regulation of Spemann organizer activity. *Cell*. 1997;91(3):407–416. PMID: 9363949. doi:10.1016/s0092-8674(00)80424-9.
  6. Plouhinec JL, Zakin L, Moriyama Y, De Robertis EM. Chordin forms a self-organizing morphogen gradient in the extracellular space between ectoderm and mesoderm in the *Xenopus* embryo. *Proc Natl Acad Sci USA*. 2013;110(51):20372–20379. PMID: 24284174. doi:10.1073/pnas.1319745110.
  7. Bier E, De Robertis EM. BMP gradients: a paradigm for morphogen-mediated developmental patterning. *Science*. 2015;348(6242):aaa5838. PMID: 26113727. doi:10.1126/science.aaa5838.
  8. Moser M, Binder O, Wu Y, Aitsebaomo J, Ren R, Bode C, Bautch VL, Conlon FL, Patterson C. BMPER, a novel endothelial cell precursor-derived protein, antagonizes bone morphogenetic protein signaling and endothelial cell differentiation. *Mol Cell Biol*. 2003;23(16):5664–5679. PMID: 12897139. doi:10.1128/MCB.23.16.5664-5679.2003.
  9. Ambrosio AL, Taelman VF, Lee HX, Metzinger CA, Coffinier C, De Robertis EM. Crossveinless-2 is a BMP feedback inhibitor that binds Chordin/BMP to regulate *Xenopus* embryonic patterning. *Dev Cell*. 2008;2(2):248–260. PMID: 18694564. doi:10.1016/j.devcel.2008.06.013.
  10. O'Connor MB, Umulis D, Othmer HG, Blair SS. Shaping BMP morphogen gradients in the *Drosophila* embryo and pupal wing. *Development*. 2006;133(2):183–193. PMID: 16368928. doi:10.1242/dev.02214.
  11. Conley CA, Silburn R, Singer MA, Ralston A, Rohwer-Nutter D, Olson DJ, Gelbart W, Blair SS. Crossveinless 2 contains cysteine-rich domains and is required for high levels of BMP-like activity during the formation of the cross veins in *Drosophila*. *Development*. 2000;127(18):3947–3959. PMID: 10952893. doi:10.1242/dev.127.18.3947.
  12. Zakin L, Metzinger CA, Chang EY, Coffinier C, De Robertis EM. Development of the vertebral morphogenetic field in the mouse: interactions between Crossveinless-2 and Twisted Gastrulation. *Dev Biol*. 2008;323(1):6–18. PMID: 18789316. doi:10.1016/j.ydbio.2008.08.019.
  13. Thul PJ, Lindskog C. The human protein atlas: a spatial map of the human proteome. *Protein Sci*. 2018;27(1):233–244. PMID: 28940711. doi:10.1002/pro.3307.
  14. Tomczak K, Czerwińska P, Wiznerowicz M. The Cancer Genome Atlas (TCGA): an immeasurable source of knowledge. *Contemp Oncol (Pozn)*. 2015;19(1A):A68–77. PMID: 25691825. doi:10.5114/wo.2014.47136.
  15. Cerami E, Gao J, Dogrusoz U, Gross BE, Sumer SO, Aksoy BA, Jacobsen A, Byrne CJ, Heuer ML, Larsson E, et al. The cBio cancer genomics portal: an open platform for exploring multidimensional cancer genomics data. *Cancer Discov*. 2012;2(5):401–404. PMID: 22588877. doi:10.1158/2159-8290.CD-12-0095.
  16. Tsherniak A, Vazquez F, Montgomery PG, Weir BA, Kryukov G, Cowley GS, Gill S, Harrington WF, Pantel S, Krill-Burger JM, et al. Defining a Cancer Dependency Map. *Cell*. 2017;170(3):564–576. e16. PMID: 28753430. doi:10.1016/j.cell.2017.06.010.
  17. Consortium G, Thomas J, Salvatore M, Phillips R, Lo E, Shad S, Hasz R, Walters G, Garcia F, Young N, et al. The Genotype-Tissue Expression (GTEx) project. *Nat Genet*. 2013;45(6):580–585. PMID: 23715323. doi:10.1038/ng.2653.
  18. GeneBio Systems, Inc. Human Chordin (CHRD) ELISA kit. Ontario (CA): GeneBio Systems, Inc.; 2011 [accessed 2022 Dec 4]. <https://www.genebiosystems.com/products/human-chordinchrd-elisa-kit>
  19. Lehallier B, Gate D, Sghaum N, Nanasi T, Lee SE, Yousef H, Losada PM, Berdnik D, Keller A, Veghese J, et al. Undulating changes in human plasma proteome profiles across the lifespan. *Nat Med*. 2019;26:1843–1850. PMID: 31806903. doi:10.1038/s41591-019-0673-2.
  20. Millet C, Lemaire P, Orsetti B, Guglielmi P, François V. The human chordin gene encodes several differentially expressed spliced variants with distinct BMP opposing activities. *Mech Dev*. 2001;106(1–2):85–96. PMID: 11472837. doi:10.1016/s0925-4773(01)00423-3.
  21. Friedman SL. Hepatic stellate Cells: protean, multifunctional, and enigmatic cells of the liver *Physiol. Rev*. 2008;88(1):125–172. PMID:18195085. doi:10.1152/physrev.00013.2007.
  22. Cyr-Depauw C, Northey JJ, Tabariés S, Annis MG, Dong Z, Cory S, Hallett M, Rennhack JP, Andrechek ER, Siegel PM. Chordin-Like 1 Suppresses Bone Morphogenetic Protein 4-Induced Breast Cancer Cell Migration and Invasion. *Mol Cell Biol*. 2016;36(10):1509–1525. PMID: 26976638. doi:10.1128/MCB.00600-15.
  23. Moll F, Millet C, Noël D, Orsetti B, Bardin A, Katsaros D, Jorgensen C, Garcia M, Theillet C, Pujol P, et al. Chordin is under-expressed in ovarian tumors and reduces tumor cell motility. *Faseb J*. 2006;20(2):240–250. PMID: 16449796. doi:10.1096/fj.05-4126com.
  24. Deng B, Chen X, Xu L, Zheng L, Zhu X, Shi J, Yang L, Wang D, Jiang D. Chordin-like 1 is a novel prognostic biomarker and correlative with immune cell infiltration in lung adenocarcinoma. *Aging*. 2022;14(1):389–409. PMID: 35021154. doi:10.18632/aging.203814.
  25. Wang L, Xu W, Mei Y, Wang X, Liu W, Zhu Z, Ni Z. CHRDL2 promotes cell proliferation by activating the YAP/TAZ signaling pathway in gastric cancer. *Free Radic Biol Med*. 2022;20(193):158–170. PMID: 36206931. doi:10.1016/j.freeradbiomed.2022.09.006.
  26. Wickham H. *Ggplot2: elegant graphics for data analysis*. Springer-Verlag New York; 2016.
  27. R-Studio Team. *Rstudio: integrated development for R*. Ver. 7.2.576. [RStudio]. Boston (MA): PBC; 2022 Dec 12.
  28. Love MI, Huber W, Anders S. Moderated estimation of fold change and dispersion for RNA-seq data with DESeq2. *Genome Biol*. 2014;15(12):550. PMID: 25516281. doi:10.1186/s13059-014-0550-8.
  29. Spitzer M, Wildenhain J, Rappsilber J, Tyers M. BoxPlotR: a web tool for generation of box plots. *Nat Methods*. 2014;11(2):121–122. PMID: 24481215. doi:10.1038/nmeth.2811.
  30. MacParland SA, Liu JC, Ma XZ, Innes BT, Bartczak AM, Gage BK, Manuel J, Khuu N, Echeverri J, Linares I, et al. Single cell RNA sequencing of human liver reveals distinct intrahepatic macrophage populations. *Nat Commun*. 2018;9(1):4383. PMID: 30348985. doi:10.1038/s41467-018-06318-7.
  31. Becht E, McInnes L, Healy J, Dutertre CA, Kwok IWH, Ng LG, Ginhoux F, Newell EW. Dimensionality reduction for visualizing single-cell data using UMAP. *Nat Biotechnol*. 2018. PMID: 30531897. doi:10.1038/nbt.4314.